

# Performance Analysis of OTSM under Hardware Impairments in Millimeter-Wave Vehicular Communication Networks

Abed Doosti-Aref, *Member, IEEE*, Sapta Girish Neelam, *Member, IEEE*, P. R. Sahu, *Member, IEEE*, Xu Zhu, *Senior Member, IEEE*, Ertugrul Basar, *Fellow, IEEE*, Sinem Coleri, *Fellow, IEEE*, and Huseyin Arslan, *Fellow, IEEE*

**Abstract**—Orthogonal time sequence multiplexing (OTSM) has been recently proposed as a single-carrier (SC) waveform offering similar bit error rate (BER) to multi-carrier orthogonal time frequency space (OTFS) modulation in doubly-spread channels under high mobilities; however, with much lower complexity making OTSM a promising candidate for low-power millimeter-wave (mmWave) vehicular communications in 6G wireless networks. In this paper, the performance of OTSM-based homodyne transceiver is explored under hardware impairments (HIs) including in-phase and quadrature imbalance (IQI), direct current offset (DCO), phase noise, power amplifier non-linearity, carrier frequency offset, and synchronization timing offset. First, the discrete-time baseband signal model is obtained in vector form under the mentioned HIs. Then, the system input-output relations are derived in time, delay-time, and delay-sequency (DS) domains in which the parameters of HIs are incorporated. Analytical studies demonstrate that noise stays white Gaussian and effective channel matrix is sparse in the DS domain under HIs. Also, DCO appears as a DC signal at receiver interfering with only the zero sequency over all delay taps in the DS domain; however, IQI redounds to self-conjugated fully-overlapping sequency interference. Simulation results reveal the fact that with no HI compensation (HIC), not only OTSM outperforms plain SC waveform but it performs close to uncompensated OTFS system; however, HIC is essentially needed for OTSM systems operating in mmWave and beyond frequency bands.

**Index Terms**—OTSM, Delay-sequency domain, Hardware impairment, IQ imbalance, Direct current offset, Phase noise, Power amplifier nonlinearity, Carrier frequency offset, Synchronization timing offset.

## I. INTRODUCTION

The sixth generation (6G) of wireless networks is characterized by the new technologies aiming at supporting higher reliability, power efficiency, and spectral efficiency in vehicular things communication networks (VTCNs) with high mobilities [1]. To accommodate the mentioned demands and bandwidth shortage, millimeter-wave (mmWave) and beyond frequency bands are employed; however, hardware impairments (HIs) are challenging issues in such frequency bands and evaluation the performance of candidate waveforms

under HIs is therefore an essential design step [2]–[5].

Orthogonal time sequence multiplexing (OTSM) has been recently proposed as a promising single-carrier (SC) waveform in delay-sequency (DS) domain [6], [7] which offers similar BER to orthogonal time frequency space (OTFS) modulation [8]; however, with much lower complexity in doubly spread channels (DSCs) under high mobilities. Since OTSM is based on Walsh-Hadamard transform (WHT), the modulation and demodulation in OTSM-based systems are merely implemented through the addition and subtraction operations, which give rise to much lower implementation complexity compared to other transform domains implemented through multiplication operation. Such superiorities make OTSM a potential candidate and the OTSM-based transceivers as affordable communication equipment for low-power SC communications in mmWave and beyond 6G-VTCNs [1], [5]–[7].

Homodyne transceivers suit the implementation limitations in VTCNs rather than heterodyne configuration imposing extra complexity and energy consumption to the system [2]. However, homodyne direct conversion transceivers suffer from HIs, such as phase noise (PN) [2]–[4], [9], [10], in-phase and quadrature imbalance (IQI) [2], [10]–[22], and direct current offset (DCO) [20] happening at both transmitter (Tx) and receiver (Rx), power amplifier non-linearity (PAN) [14], [15], [18] occurring at Tx along with carrier frequency offset (CFO) [2], [9], [22], [23] and synchronization timing offset (STO) [9], [22], [23] betiding at Rx. Such impairments are mainly due to the fabrication inaccuracies of analog components, which give rise to performance degradation and energy inefficiency [2]. To evaluate the robustness of waveforms under HIs and propose practical breakthroughs for HI compensation (HIC), obtaining the system input-output (I/O) relation by incorporating the HIs parameters is a prerequisite design step since it alters for narrowband (NB) and wideband (WB) applications in time-frequency, delay-Doppler (DD), delay-scale, and DS domains [13]–[25].

From the HIs point of view, OFDM and OTFS have been well studied in the literature [2]–[5], [9]–[23]. However, the number of works on HIs in OTSM-based systems is sporadic [24], [25]. In [24], the I/O relation is first obtained for OTSM systems under HIs by considering only frequency-independent IQI, which can be also named as NB-IQI at Rx and then an embedded pilot arrangement is presented for joint HIC and channel parameters estimation. In [25], the I/O relation is derived for OTSM homodyne transceivers under only NB-IQI

Abed (Abdollah) Doosti-Aref is with Sharif University of Technology, [a.doosti@sharif.edu](mailto:a.doosti@sharif.edu). Sapta Girish Neelam, [sgn10@iitbbs.ac.in](mailto:sgn10@iitbbs.ac.in), and Pravas Ranjan Sahu, [prs@iitbbs.ac.in](mailto:prs@iitbbs.ac.in) are with IIT Bhubaneswar. Xu Zhu is with Harbin Institute of Technology, [xuzhu@ieee.org](mailto:xuzhu@ieee.org). Ertugrul Basar, [ebasar@ku.edu.tr](mailto:ebasar@ku.edu.tr), and Sinem Coleri, [scoleri@ku.edu.tr](mailto:scoleri@ku.edu.tr), are with Koc University. Huseyin Arslan is with Istanbul Medipol University, [huseyinarslan@medipol.edu.tr](mailto:huseyinarslan@medipol.edu.tr).

at both Tx and Rx through which the training sequence is employed for joint HIC and channel parameters estimation. To the best of the authors knowledge, the I/O relation and performance evaluation of OTSM systems in the presence of DCO, PAN, PN, CFO, and STO have not been yet addressed in the literature.

Motivated by this background, the main contributions in this paper are summarized as follows.

- i) We propose a discrete-time baseband signal model for OTSM homodyne transceiver in vector form through which the components of different HIs are incorporated independently and step by step to the signal and system models. In this context, we consider the memory effects of PAN at Tx, IQI, DCO, and PN at both Tx and Rx, along with CFO and STO at Rx. The proposed model can be utilized in VTCNs for vehicle-to-vehicle, vehicle-to-base station, and high-speed train-to-vehicle communication links, which are equipped with homodyne transceivers.
- ii) The system I/O relations are obtained in time, delay-time (DT), and DS domains in both vector and matrix forms by incorporating Tx/Rx IQI, Tx/Rx DCO, Tx/Rx PN, PAN, CFO, and STO. In particular, it will be demonstrated that the I/O relations presented in [12], [24], and [25] are derived as the special cases from our proposed comprehensive model.
- iii) Analytical studies demonstrate that although the received noise is imposed by IQI, PN, and CFO at the Rx, its additive white Gaussian property is retained in the DS domain. Also, the effective channel matrix in DS domain is sparse under HIs. Moreover, IQI in OTSM transceivers redounds to self-conjugated sequency interference (SCSI) of the channel impaired symbols along all their sequencies; however, DCO introduces only the zero sequency interference (ZSI) over all delay taps.
- iv) Extensive simulation studies are carried out to evaluate the performance of OTSM in the presence of Tx/Rx IQI, Tx/Rx DCO, Tx/Rx PN, PAN, CFO, and STO in VTCNs for different mobility speeds, modulation orders, and detectors. To show the necessity of addressing HIC in OTSM-based systems by exploiting the prerequisites presented in this paper as the next step of this study, we further compare the performance of OTSM under HIs with an ideal system including no HIs, plain SC-waveform under HIs, and the analogous OTFS system in which all mentioned HIs have been appropriately compensated through the recently-proposed HIC schemes for OTFS-based system.

The notations used in this paper are as follows. Boldface uppercase and lowercase letters represent the matrices and column vectors, respectively.  $\mathcal{CN}(\mu_0, \sigma_0^2)$  denotes the complex normal distribution with mean  $\mu_0$  and variance  $\sigma_0^2$ .  $\mathbf{W}_N$ ,  $\mathbf{I}_N$ ,  $\mathbf{1}_N$ , and  $\mathbf{0}_N$  represent the normalized  $N$ -point WHT square matrix,  $N$ -square identity matrix, all-ones, and all-zeros column vectors of length  $N$ , respectively. Let  $(\cdot)^*$ ,  $(\cdot)^T$ ,  $(\cdot)^H$ , and  $\delta(\cdot)$  stand for the complex conjugate, transpose, Hermitian transpose, and Dirac delta function, respectively.  $\mathbb{C}^{M \times N}$  denotes the set of  $M \times N$  dimensional matrices with

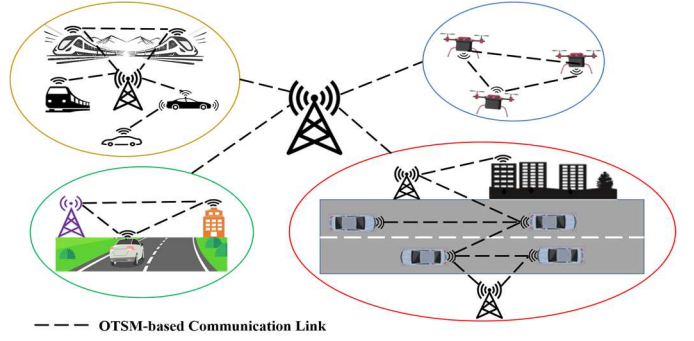


**Fig. 1.** Illustration of vehicular things in the VTCN model used in this paper.

complex entries,  $\text{cov}(\mathbf{a})$  the covariance matrix of vector  $\mathbf{a}$ ,  $\text{vec}(\mathbf{A})$  the column-wise vectorization of matrix  $\mathbf{A}$ , and  $\text{vec}_{M,N}^{-1}(\mathbf{a})$  an  $M \times N$  dimensional matrix, which is folded column-wise from the column vector  $\mathbf{a}$  of length  $NM$ . Let  $\otimes$  stand for the Kronecker product,  $\odot$  for the Hadamard product, and  $\boxtimes$  for the dyadic convolution.

The rest of the paper is organized as follows. The system model is described in Section II followed by the OTSM transceiver signal model under HIs presented in Section III. Derivation of I/O relations in time, DT, and DS domains along with the associated discussions are presented in Section IV. Performance evaluation is provided in Section V. Finally, conclusion and future insights are summarized in Section VI.

## II. SYSTEM MODEL

We consider a VTCN including vehicles moving at different speeds, base stations located at different places of the network, high-speed trains, and other fixed and mobile users as shown in Fig. 1. The reason for selecting a VTCN is to evaluate the performance of OTSM with respect to the attributes of time-varying DSC under high mobilities, which is one of the envisaged channels in the 6G wireless networks.

All vehicles are equipped with an OTSM-based homodyne transceiver enabling communication to everything (V2X) in VTCN as depicted in Fig. 1. For each vehicle in the VTCN, single antenna is adopted to emit the information symbols, which are independent and identically distributed with zero mean. The quadrature amplitude modulation (QAM) mapping is utilized to decorate  $M \times N$  symbols in the DS domain as an OTSM frame, where  $M$  and  $N$  denote the number of delay and sequency bins of the DS grid, respectively.  $N$  is considered to be a power of 2 and each OTSM frame occupies a bandwidth of  $B = M\Delta f$  Hz and a time duration of  $T_f = NT$  seconds, where  $\Delta f$  and  $T$  denote the sampling frequency interval and symbol duration, respectively. Also, we have the constraint  $T\Delta f = 1$ , i.e., the area of delay-sequency box for each OTSM frame in DS grid is equal to one enabling critical sampling for any pulse shaping waveform.

A time-varying DSC model with  $P$  dominant reflectors is adopted to represent the channel for each V2X link in the VTCN. Accordingly, the channel impulse response (CIR) in DD domain has a sparse configuration which is given as

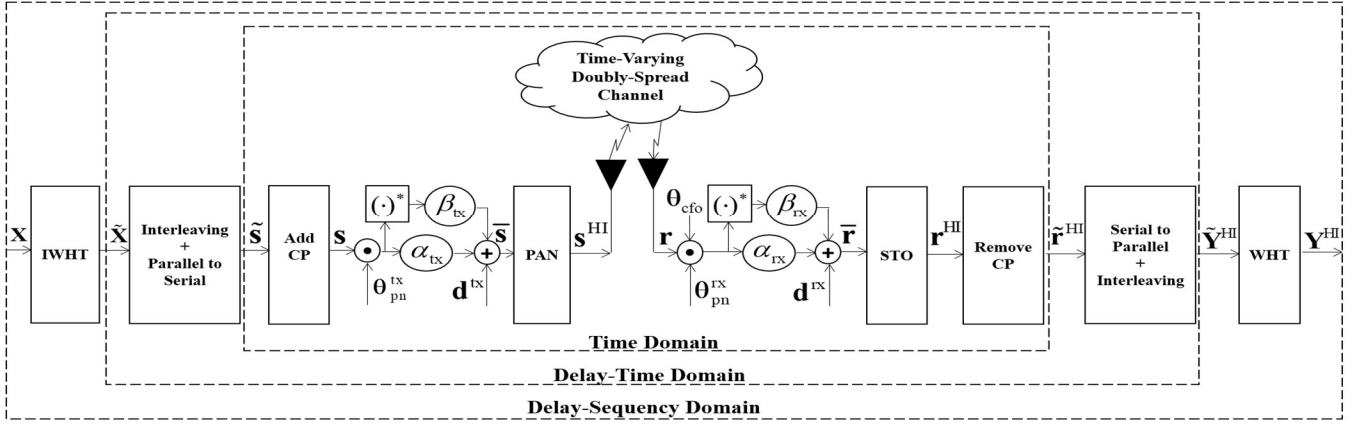


Fig. 2. The block diagram of OTSM transceiver for each V2X link in the presence of Tx/Rx HIs.

$$h(\tau, \nu) = \sum_{i=1}^P h_i \delta(\tau - \tau_i) \delta(\nu - \nu_i), \quad (1)$$

where  $h_i \sim \mathcal{CN}(0, \sigma_{h_i}^2)$ ,  $0 \leq \tau_i \leq \tau_{\max}$ , and  $-\nu_{\max} \leq \nu_i \leq \nu_{\max}$  denote the propagation gain, fractional delay shift, and fractional Doppler shift associated with the  $i^{\text{th}}$  channel path, respectively. Also,  $\ell_i = \tau_i B \in \mathbb{R}$  and  $k_i = \nu_i T_f \in \mathbb{R}$  denote the normalized delay shift and normalized Doppler shift related to the  $i^{\text{th}}$  channel path, respectively. Thus,  $\ell_{\max}$  and  $k_{\max}$  represent the maximum delay and Doppler shift indices of the channel, respectively. Accordingly,  $\tau_{\max}$  and  $\nu_{\max}$  represent the maximum delay and Doppler shift of the channel, which are constrained as  $\tau_{\max} \nu_{\max} \ll 1$ , i.e., under spread fading channel. Applying inverse fast Fourier transform to the Doppler dimension in (1), the CIR in DT domain is obtained as

$$g(\tau, t) = \int_{\nu} h(\tau, \nu) e^{j2\pi\nu(t-\tau)} d\nu = \sum_{i=1}^P h_i e^{j2\pi\nu_i(t-\tau_i)}. \quad (2)$$

Let  $\mathcal{L} = \{0, \dots, l_{\max}\}$  be the set of discrete delay bins describing delay shifts at integer multiples of the delay resolution  $1/M\Delta f$ . After applying sampling theorem to  $g(\tau, t)$  at integer multiples of the delay resolution, namely  $t = q/M\Delta f$  for  $q = 0, \dots, NM + l_{\max} - 1$  and  $\tau = l/M\Delta f$  for  $l \in \mathcal{L}$ , the discrete-time baseband CIR in DT domain is given as

$$g[l, q] = \sum_{i=1}^P h_i e^{j2\pi k_i(q-l)/MN} \text{sinc}(l - \ell_i), \quad (3)$$

where  $\text{sinc}(x) = \sin(\pi x)/(\pi x)$  [26], [27].

### III. OTSM TRANSCEIVER SIGNAL MODEL UNDER HIS

This section aims at obtaining the vector form signal model for the OTSM transceiver under IQI, DCO, PN, memory effects of PAN, CFO, and STO based on the block diagram depicted in Fig. 2.

#### A. OTSM Transmitted Frame Before Incorporating Tx-HIs

Let  $\mathbf{x} \in \mathbb{C}^{NM \times 1} = [\mathbf{x}_0^T, \dots, \mathbf{x}_{M-1}^T]^T$  be the vector of information symbols in DS domain, where the symbol vectors  $\mathbf{x}_m \in \mathbb{C}^{N \times 1}$  for  $m = 0, \dots, M-1$  correspond to the DS matrix representation of information symbols given as  $\mathbf{X} \in \mathbb{C}^{M \times N} = [\mathbf{x}_0, \dots, \mathbf{x}_{M-1}]^T$  after

standing at each row of  $\mathbf{X}$  to have  $\mathbf{x} = \text{vec}(\mathbf{X}^T)$ . Accordingly, the row and column indices of  $\mathbf{X}$  correspond to the delay and sequency indices of the DS grid, respectively. To prevent inter block interference (IBI) and interference between the data and pilots, the last  $2l_{\max} + 1$  rows of  $\mathbf{X}$  are set to zero enabling interleaved zero padding (ZP) among the blocks [7]. Not only does this setting guard the tandem leakage but also facilitate the channel estimation in time domain [7]. As depicted in Fig. 2, to move from DS domain to DT domain, an  $N$ -point inverse WHT (IWHT) is applied along the sequency dimension, namely each row of  $\mathbf{X}$  as

$$\tilde{\mathbf{X}} = [\tilde{\mathbf{x}}_0, \dots, \tilde{\mathbf{x}}_{M-1}]^T = \mathbf{X} \mathbf{W}_N. \quad (4)$$

Defining  $\tilde{\mathbf{x}} \in \mathbb{C}^{NM \times 1} = [\tilde{\mathbf{x}}_0^T, \dots, \tilde{\mathbf{x}}_{M-1}^T]^T$  as the input of DT domain, we have  $\tilde{\mathbf{x}} = \text{vec}(\tilde{\mathbf{X}}^T)$ . The DT samples are then column-wise vectorized to generate the time domain samples vector  $\tilde{\mathbf{s}} = \text{vec}(\tilde{\mathbf{X}})$ , which is further burst into  $N$  blocks each of which of length  $M$  in time domain as  $\tilde{\mathbf{s}} \in \mathbb{C}^{NM \times 1} = [\tilde{\mathbf{s}}_0^T, \dots, \tilde{\mathbf{s}}_{N-1}^T]^T$ . The vector representation of  $\tilde{\mathbf{X}}$  gives rise to the interleaved transmission of the information symbols in time domain, which can be readily represented in terms of  $\tilde{\mathbf{x}}$  and the interleave perfect shuffle matrix  $\mathbf{P}$  as

$$\tilde{\mathbf{s}} = \mathbf{P} \tilde{\mathbf{x}}. \quad (5)$$

Consequently, due to row-column interleaving, the  $M$  samples of the time domain blocks  $\tilde{\mathbf{s}}_n$  correspond to the DT symbol vectors  $\tilde{\mathbf{x}}_m$  as  $\tilde{\mathbf{s}}_n[m] = \tilde{\mathbf{x}}_m[n]$ . This relation will be utilized in Subsection IV. B to obtain the I/O relation in DT domain.

To represent  $\tilde{\mathbf{s}}$  as the input of time domain channel in terms of  $\mathbf{x}$  as the input of DS domain channel, we use the relation between the column-wise vectorization and Kronecker product. Considering the equation  $\mathbf{V} = \mathbf{A} \mathbf{X} \mathbf{B}$ , where  $\mathbf{V}$ ,  $\mathbf{A}$ ,  $\mathbf{X}$ , and  $\mathbf{B}$  are given matrices, a more convenient form can be represented as

$$\text{vec}(\mathbf{V}) = (\mathbf{B}^T \otimes \mathbf{A}) \text{vec}(\mathbf{X}). \quad (6)$$

When we apply this to (4) while using the relation between the perfect shuffle matrix  $\mathbf{P}$  and column-wise vectorization for a given matrix  $\mathbf{C}$ , i.e.,  $\text{vec}(\mathbf{C}) = \mathbf{P} \text{vec}(\mathbf{C}^T)$ , the transmitted vector in time domain in terms of the vector of information symbols in DS domain can be rewritten as

$$\tilde{\mathbf{s}} = (\mathbf{W}_N \otimes \mathbf{I}_M) \mathbf{P} \mathbf{x}. \quad (7)$$

Also, by using the property of the unitary permutation matrix  $\mathbf{P}$  for given square matrices  $\mathbf{I}_M$  and  $\mathbf{W}_N$  i.e.,  $(\mathbf{I}_M \otimes \mathbf{W}_N) = \mathbf{P}(\mathbf{W}_N \otimes \mathbf{I}_M) \mathbf{P}^T$ , (7) can be rewritten as

$$\tilde{\mathbf{s}} = \mathbf{P}(\mathbf{I}_M \otimes \mathbf{W}_N) \mathbf{x}. \quad (8)$$

To aid the channel estimation process, as depicted in Fig. 2, a cyclic prefix (CP) of length  $l_{\max}$  is copied from the end of the time domain vector and appended as a preamble at the head of the vector, which is given as

$$\mathbf{s} \in \mathbb{C}^{(NM+l_{\max}) \times 1} = \mathbf{A}_{\text{cp}} \tilde{\mathbf{s}}, \quad (9)$$

where  $\mathbf{A}_{\text{cp}} \in \mathbb{R}^{(NM+l_{\max}) \times NM} = \begin{bmatrix} \mathbf{0}_{l_{\max} \times (NM-l_{\max})} & \mathbf{I}_{l_{\max}} \\ & \mathbf{I}_{NM} \end{bmatrix}$  denotes the CP insertion matrix.

### B. OTSM Transmitted Frame After Incorporating Tx-HIs

In the presence of IQI, DCO, and PN at Tx, as depicted in Fig. 2, the time domain impaired vector  $\bar{\mathbf{s}}$  can be mathematically modeled as

$$\bar{\mathbf{s}} = \alpha_{\text{tx}} (\mathbf{s} \odot \boldsymbol{\theta}_{\text{pn}}^{\text{tx}}) + \beta_{\text{tx}} (\mathbf{s} \odot \boldsymbol{\theta}_{\text{pn}}^{\text{tx}})^* + \mathbf{d}^{\text{tx}}, \quad (10)$$

where  $\mathbf{d}^{\text{tx}} \in \mathbb{R}^{(NM+l_{\max}) \times 1} = d^{\text{tx}} \mathbf{1}_{NM+l_{\max}}$  denotes the DCO at Tx. We assume the practical asymmetrical model through which the Tx-IQI coefficients are given as  $\alpha_{\text{tx}} = (1 + g_{\text{tx}} e^{-j\varphi_{\text{tx}}/2})/2$  and  $\beta_{\text{tx}} = (1 - g_{\text{tx}} e^{j\varphi_{\text{tx}}/2})/2$ , where  $g_{\text{tx}}$  and  $\varphi_{\text{tx}}$  represent the gain and phase mismatch, respectively. In addition, the oscillator output at Tx with carrier frequency of  $f_c$  and PN process of  $\theta_{\text{pn}}^{\text{tx}}(t)$  is modeled as  $e^{-j(2\pi f_c t + \theta_{\text{pn}}^{\text{tx}}(t))}$  [2]. Accordingly, the Tx-PN process sampled at  $t = q/M\Delta f$  for  $q = 0, \dots, NM+l_{\max}-1$  in the discrete-time equivalent baseband model can be given as  $S_{\text{pn}}^{\text{tx}}[q] = e^{-j\theta_{\text{pn}}^{\text{tx}}[q]}$ . Consequently, the Tx-PN vector  $\boldsymbol{\theta}_{\text{pn}}^{\text{tx}}$  in (10) is given as

$$\boldsymbol{\theta}_{\text{pn}}^{\text{tx}} \in \mathbb{C}^{(NM+l_{\max}) \times 1} = [S_{\text{pn}}^{\text{tx}}[0], \dots, S_{\text{pn}}^{\text{tx}}[NM+l_{\max}-1]]^T. \quad (11)$$

To incorporate PAN and memory effects with the signal vector at Tx, we assume memory polynomial based on the complexity-reduced Volterra model, which includes memory effects and exponentiated envelope terms [14], [15]. Accordingly, by considering  $\bar{\mathbf{s}}[q]$  as the input of power amplifier (PA) as shown in Fig. 2, the discrete baseband samples of hardware impaired vector  $\mathbf{s}^{\text{HI}}$  at the output of PA under Tx-IQI, Tx-DCO, Tx-PN, and PAN are obtained by

$$\mathbf{s}^{\text{HI}}[q] = \sum_{j=0}^{N_\rho-1} \sum_{i=0}^{M_\rho} \rho_{ij} \bar{\mathbf{s}}[q-i] \bar{\mathbf{s}}[q-i]^j, \quad (12)$$

where  $\rho_{ij}$ ,  $M_\rho$ , and  $N_\rho$  denote the linearization coefficients, non-linear memory depth, and non-linearity order, respectively [14], [15].

Finally, after pulse shaping of time domain samples  $\mathbf{s}^{\text{HI}}[q]$  followed by digital to analog converter, the hardware impaired analog signal  $S^{\text{HI}}(t)$  is transmitted to the time-varying DSC as depicted in Fig. 2.

### C. OTSM Received Frame Before Incorporating Rx-HIs

The channel impaired signal at Rx is given as  $r(t) = \int_0^{t_{\max}} g(\tau, t) s^{\text{HI}}(t-\tau) d\tau + w(t)$ , where the additive noise  $w(t)$  is distributed as  $\mathcal{CN}(0, \sigma_0^2)$ . Sampling  $r(t)$  with a time

period of  $T_s = 1/M\Delta f$  at  $t = qT_s$  for  $q = 0, \dots, NM+l_{\max}-1$ , the discrete-time baseband channel impaired signal in time domain can be readily written as

$$\mathbf{r}[q] = \sum_{l \in \mathcal{L}} g[l, q] \mathbf{s}^{\text{HI}}[q-l] + \mathbf{w}[q], \quad (13)$$

where  $\mathbf{w}$  is considered to be a Gaussian random vector with  $\text{cov}(\mathbf{w}) = \sigma_0^2 \mathbf{I}_{NM+l_{\max}}$ .

### D. OTSM Received Frame After Incorporating IQI, DCO, PN, and CFO at Rx

In the presence of IQI, DCO, PN, and CFO at Rx, as depicted in Fig. 2, the time domain channel impaired vector  $\bar{\mathbf{r}}$  can be mathematically modeled as

$$\bar{\mathbf{r}} = \alpha_{\text{rx}} (\mathbf{r} \odot \boldsymbol{\theta}_{\text{pn}}^{\text{rx}} \odot \boldsymbol{\theta}_{\text{cfo}}) + \beta_{\text{rx}} (\mathbf{r} \odot \boldsymbol{\theta}_{\text{pn}}^{\text{rx}} \odot \boldsymbol{\theta}_{\text{cfo}})^* + \mathbf{d}^{\text{rx}}, \quad (14)$$

where  $\mathbf{d}^{\text{rx}} \in \mathbb{R}^{(NM+l_{\max}) \times 1} = d^{\text{rx}} \mathbf{1}_{NM+l_{\max}}$  represents the Rx-DCO vector. Also  $\alpha_{\text{rx}} = (1 + g_{\text{rx}} e^{-j\varphi_{\text{rx}}/2})/2$  and  $\beta_{\text{rx}} = (1 - g_{\text{rx}} e^{j\varphi_{\text{rx}}/2})/2$

stand for the asymmetrical Rx-IQI coefficients in which  $g_{\text{rx}}$  and  $\varphi_{\text{rx}}$  represent the gain and phase imbalance at Rx, respectively. Here, we have assumed that the oscillator output at Rx with carrier frequency of  $f_c$ , CFO of  $f_o$ , and PN

process of  $\theta_{\text{pn}}^{\text{rx}}(t)$  is modeled as  $e^{-j(2\pi(f_c + f_o)t + \theta_{\text{pn}}^{\text{rx}}(t))}$  [2].

Accordingly, the PN process and the CFO phase process at Rx in the discrete-time equivalent baseband model sampled at  $t = q/M\Delta f$  for  $q = 0, \dots, NM+l_{\max}-1$  can be given as

$S_{\text{pn}}^{\text{rx}}[q] = e^{-j\theta_{\text{pn}}^{\text{rx}}[q]}$  and  $S_{\text{cfo}}[q] = e^{-j2\pi f_o q}$ , respectively. Therefore,

the Rx-PN vector  $\boldsymbol{\theta}_{\text{pn}}^{\text{rx}}$  and CFO phase vector  $\boldsymbol{\theta}_{\text{cfo}}$  in (14) are given as

$$\boldsymbol{\theta}_{\text{pn}}^{\text{rx}} \in \mathbb{C}^{(NM+l_{\max}) \times 1} = [S_{\text{pn}}^{\text{rx}}[0], \dots, S_{\text{pn}}^{\text{rx}}[NM+l_{\max}-1]]^T, \quad (15)$$

$$\boldsymbol{\theta}_{\text{cfo}} \in \mathbb{C}^{(NM+l_{\max}) \times 1} = [S_{\text{cfo}}[0], \dots, S_{\text{cfo}}[NM+l_{\max}-1]]^T. \quad (16)$$

### E. OTSM Hardware Impaired Received Frame After Incorporating STO

To incorporate STO with  $\bar{\mathbf{r}}$ , we utilize the Gardner's timing synchronization loop at Rx through which the optimal symbol timing instants are estimated [22]. Accordingly, we assume the receiver samples at a rate of  $1/T_i$  at  $t = qT_i$  to obtain the samples of time domain hardware impaired received vector  $\mathbf{r}^{\text{HI}}$  under Rx-IQI, Rx-DCO, Rx-PN, CFO, and STO as

$$\mathbf{r}^{\text{HI}}[q] = \sum_{i=I_1}^{I_2} \bar{\mathbf{r}}[m_q - i] h_{\text{intp}}[i + \mu_q], \quad (17)$$

where  $I_1$  and  $I_2$  are finite integers and  $m_q$ ,  $\mu_q$ , and  $h_{\text{intp}}$  are the base-point for the  $q^{\text{th}}$  interpolant, fractional interval, and impulse response of the interpolating filter, respectively [22].

### F. OTSM Hardware Impaired Received Frame in DT and DS Domains

Let  $\mathbf{R}_{\text{cp}} \in \mathbb{R}^{NM \times (NM+l_{\max})} = [\mathbf{0}_{NM \times l_{\max}}, \mathbf{I}_{NM}]$  denote the CP removal matrix as depicted in Fig. 2. Then, the CP is removed from the time domain vector as

$$\tilde{\mathbf{r}}^{\text{HI}} \in \mathbb{C}^{NM \times 1} = \mathbf{R}_{\text{cp}} \mathbf{r}^{\text{HI}}. \quad (18)$$

As shown in Fig. 2, after removing the CP, the time domain channel impaired vector  $\tilde{\mathbf{r}}^{\text{HI}}$  is folded back into a matrix to represent the DT received matrix as  $\tilde{\mathbf{Y}}^{\text{HI}} \in \mathbb{C}^{M \times N} = \text{vec}_{M,N}^{-1}(\tilde{\mathbf{r}}^{\text{HI}}) = [\tilde{\mathbf{y}}_0^{\text{HI}}, \dots, \tilde{\mathbf{y}}_{M-1}^{\text{HI}}]^T$ . Defining  $\tilde{\mathbf{y}}^{\text{HI}} = [\tilde{\mathbf{y}}_0^{\text{HI}^T}, \dots, \tilde{\mathbf{y}}_{M-1}^{\text{HI}^T}]^T$  as the output vector of DT domain at Rx, the relation between

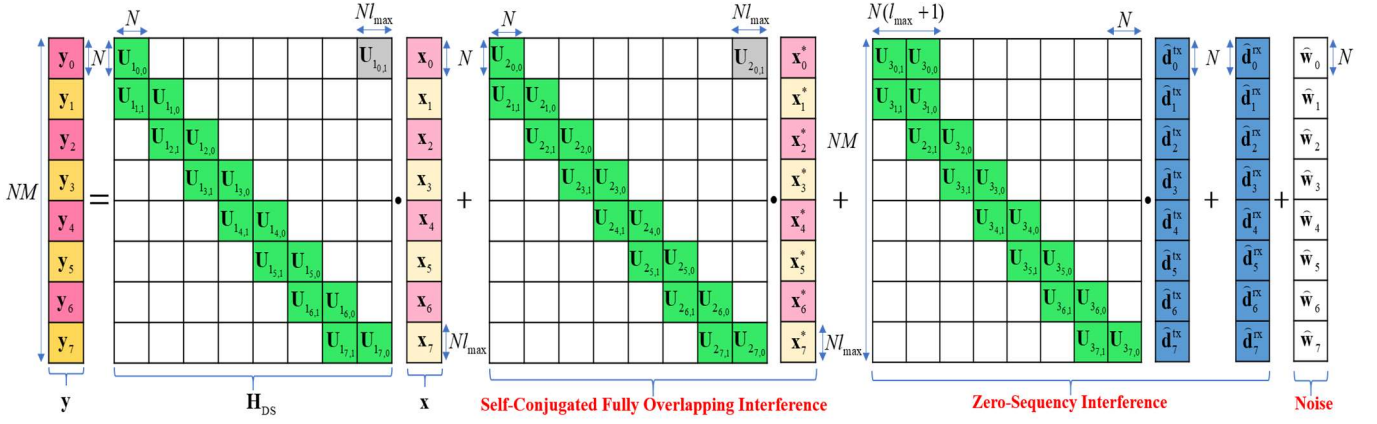


Fig. 3. Illustration of the I/O relation in DS domain for OTSM transceiver under HIs,  $N = M = 8, l_{\max} = 2$ .

$\tilde{\mathbf{r}}^{\text{HI}}$ ,  $\tilde{\mathbf{Y}}^{\text{HI}}$ , and  $\tilde{\mathbf{y}}^{\text{HI}}$  is given as

$$\tilde{\mathbf{r}}^{\text{HI}} = \text{vec}(\tilde{\mathbf{Y}}^{\text{HI}}) = \mathbf{P}\tilde{\mathbf{y}}^{\text{HI}}, \quad (19)$$

which can be also rewritten as  $\tilde{\mathbf{y}}^{\text{HI}} = \mathbf{P}^T \tilde{\mathbf{r}}^{\text{HI}}$ . Therefore, due to the column-wise folding, the  $M$  samples of blocks  $\tilde{\mathbf{r}}_m^{\text{HI}}$  are related to the DT symbol vectors  $\tilde{\mathbf{y}}_m^{\text{HI}}$  as  $\tilde{\mathbf{r}}_m^{\text{HI}}[m] = \tilde{\mathbf{y}}_m^{\text{HI}}[n]$ . This relation will be utilized in Subsection IV. B for obtaining the I/O relation in DT domain.

To move from DT domain to DS domain, as depicted in Fig. 2,  $N$ -point WHT is applied along the time dimension, namely each row of  $\tilde{\mathbf{Y}}^{\text{HI}}$ , which is given as

$$\mathbf{Y}^{\text{HI}} = [\mathbf{y}_0^{\text{HI}}, \dots, \mathbf{y}_{M-1}^{\text{HI}}]^T = \tilde{\mathbf{Y}}^{\text{HI}} \mathbf{W}_N. \quad (20)$$

Considering  $\mathbf{y}^{\text{HI}} \in \mathbb{C}^{NM \times 1} = [(\mathbf{y}_0^{\text{HI}})^T, \dots, (\mathbf{y}_{M-1}^{\text{HI}})^T]^T$  as the output vector of DS domain at Rx, the relation between  $\mathbf{Y}^{\text{HI}}$  and  $\mathbf{y}^{\text{HI}}$  in terms of the perfect shuffle matrix  $\mathbf{P}$  is written as  $\mathbf{P}\mathbf{y}^{\text{HI}} = \text{vec}(\mathbf{Y}^{\text{HI}})$ . Applying (6) to (20) and then by using  $\tilde{\mathbf{r}}^{\text{HI}} = \text{vec}(\tilde{\mathbf{Y}}^{\text{HI}})$ ,  $(\mathbf{I}_M \otimes \mathbf{W}_N) = \mathbf{P}(\mathbf{W}_N \otimes \mathbf{I}_M)\mathbf{P}^T$ , and  $\mathbf{P}\mathbf{y}^{\text{HI}} = \text{vec}(\mathbf{Y}^{\text{HI}})$ , the vector of the received symbols at the output of DS domain under HIs can be finally written as

$$\mathbf{y}^{\text{HI}} = (\mathbf{I}_M \otimes \mathbf{W}_N)\mathbf{P}^T \tilde{\mathbf{r}}^{\text{HI}}. \quad (21)$$

#### IV. SYSTEM INPUT-OUTPUT RELATIONS IN TIME, DT, AND DS DOMAINS UNDER HIS

In this section, the I/O relations in time, DT, and DS domains are derived based on the signal model for OTSM transceiver under HIs obtained in the previous section.

##### A. Vector-Form I/O Relation in Time Domain

To represent the I/O relation in terms of the delay index  $m$  and the sequency or time index  $n$  of the OTSM frame in DS or DT domains, respectively, the discrete-time index  $q$  in time domain can be separated into  $m$  and  $n$  as  $q = m + nM$ , for  $m = 0, \dots, M-1$  and  $n = 0, \dots, N-1$ . Defining  $g_1[l, m + nM]$ ,  $g_2[l, m + nM]$ ,  $g_3[l, m + nM]$ , and  $\tilde{\mathbf{w}}_n[m]$  as

$$\begin{aligned} g_1[l, m + nM] &= (\alpha_{\text{tx}} \alpha_{\text{rx}} S_{\text{pn}}^{\text{tx}}[m + nM] S_{\text{pn}}^{\text{rx}}[m + nM] S_{\text{cfo}}[m + nM] \\ &\quad g[l, m + nM] + \beta_{\text{tx}}^* \beta_{\text{rx}} S_{\text{pn}}^{\text{tx}}[m + nM] S_{\text{pn}}^{\text{rx}}[m + nM] \\ &\quad S_{\text{cfo}}[m + nM] g^*[l, m + nM]), \end{aligned} \quad (22)$$

$$\begin{aligned} g_2[l, m + nM] &= (\beta_{\text{tx}} \alpha_{\text{rx}} S_{\text{pn}}^{\text{tx}*}[m + nM] S_{\text{pn}}^{\text{rx}}[m + nM] S_{\text{cfo}}[m + nM] \\ &\quad g[l, m + nM] + \alpha_{\text{tx}}^* \beta_{\text{rx}} S_{\text{pn}}^{\text{tx}*}[m + nM] S_{\text{pn}}^{\text{rx}*}[m + nM] \\ &\quad S_{\text{cfo}}^*[m + nM] g^*[l, m + nM]), \end{aligned} \quad (23)$$

$$\begin{aligned} g_3[l, m + nM] &= (\alpha_{\text{rx}} S_{\text{pn}}^{\text{rx}}[m + nM] S_{\text{cfo}}[m + nM] g[l, m + nM] + \\ &\quad \beta_{\text{rx}} S_{\text{pn}}^{\text{rx}*}[m + nM] S_{\text{cfo}}^*[m + nM] g^*[l, m + nM]), \end{aligned} \quad (24)$$

$$\begin{aligned} \tilde{\mathbf{w}}_n[m] &= (\alpha_{\text{rx}} S_{\text{pn}}^{\text{rx}}[m + nM] S_{\text{cfo}}[m + nM] \tilde{\mathbf{w}}[m + nM] + \\ &\quad \beta_{\text{rx}} S_{\text{pn}}^{\text{rx}*}[m + nM] S_{\text{cfo}}^*[m + nM] \tilde{\mathbf{w}}^*[m + nM]), \end{aligned} \quad (25)$$

and by substituting (13) in (14), then (14) in (17), and then after removing the CP by (18), the I/O relation in time domain is obtained as

$$\begin{aligned} \tilde{\mathbf{r}}_n^{\text{HI}}[m] &= \sum_{l \in \mathcal{L}} g_1[l, m + nM] \tilde{\mathbf{s}}_n[m - l] + g_2[l, m + nM] \tilde{\mathbf{s}}_n^*[m - l] + \\ &\quad g_3[l, m + nM] \tilde{\mathbf{d}}_n^{\text{tx}}[m] + \tilde{\mathbf{d}}_n^{\text{rx}}[m] + \tilde{\mathbf{w}}_n[m]. \end{aligned} \quad (26)$$

It is worth mentioning that in (26) we have used the expressions  $\tilde{\mathbf{d}}^{\text{tx}} = \mathbf{R}_{\text{cp}} \mathbf{d}^{\text{tx}} = \mathbf{d}^{\text{tx}} \mathbf{1}_{NM}$  and  $\mathbf{d}^{\text{tx}} = \mathbf{A}_{\text{cp}} \tilde{\mathbf{d}}^{\text{tx}}$ , where  $\tilde{\mathbf{d}}^{\text{tx}} = \mathbf{d}^{\text{tx}} \mathbf{1}_{NM}$ , to obtain the I/O relation for the input of the system before inserting the CP and the output of the system after removing the CP in time domain as shown in Fig. 2.

##### B. Vector-Form I/O Relation in DT Domain

By replacing  $\tilde{\mathbf{r}}_n^{\text{HI}}[m]$  with  $\tilde{\mathbf{y}}_m^{\text{HI}}[n]$ ,  $\tilde{\mathbf{s}}_n[m]$  with  $\tilde{\mathbf{x}}_m[n]$ , and  $g_i[l, m + nM]$  with  $\tilde{\mathbf{g}}_{i,m,n}[n]$  for  $i = 1, 2, 3$  in (26), the I/O relation in DT domain is obtained as

$$\tilde{\mathbf{y}}_m^{\text{HI}}[n] = \sum_{l \in \mathcal{L}} \tilde{\mathbf{g}}_{1,m,n}[n] \tilde{\mathbf{x}}_{m-1}[n] + \tilde{\mathbf{g}}_{2,m,n}[n] \tilde{\mathbf{x}}_{m-1}^*[n] + \tilde{\mathbf{g}}_{3,m,n}[n] \tilde{\mathbf{d}}_m^{\text{tx}}[n] + \tilde{\mathbf{d}}_m^{\text{rx}}[n] + \tilde{\mathbf{w}}_m[n]. \quad (27)$$

##### C. Matrix-Form I/O Relation in Terms of Sequency Spread Matrix in DS Domain

To obtain the I/O relation in DS domain, we apply  $N$ -point WHT along the time dimension of the DT received vector in (27), i.e., each row of the DT matrix  $\tilde{\mathbf{Y}}^{\text{HI}}$  obtained through (27) for  $n = 0, \dots, N-1$ . Then, by using the multiplication property of WHT, i.e.,  $\mathbf{W}_N \cdot (\mathbf{a} \odot \mathbf{b}) = (\mathbf{W}_N \cdot \mathbf{a}) \boxtimes (\mathbf{W}_N \cdot \mathbf{b})$  for two arbitrary given vectors  $\mathbf{a}$  and  $\mathbf{b}$  of length  $N$ , the I/O relation in DS domain is obtained as

$$\begin{aligned}
\mathbf{y}^{\text{HI}} = & \underbrace{[(\mathbf{I}_M \otimes \mathbf{W}_N) \mathbf{P}^T (\alpha_{\text{tx}} \alpha_{\text{rx}} \mathbf{R}_{\text{cp}} \Theta_{\text{pn}}^{\text{rx}} \Theta_{\text{cfo}}^{\text{rx}} \mathbf{H} \Theta_{\text{pn}}^{\text{tx}} \mathbf{A}_{\text{cp}} + \beta_{\text{tx}}^* \beta_{\text{rx}} \mathbf{R}_{\text{cp}} \Theta_{\text{pn}}^{\text{rx}} \Theta_{\text{cfo}}^* \mathbf{H}^* \Theta_{\text{pn}}^{\text{tx}} \mathbf{A}_{\text{cp}}) \mathbf{P} (\mathbf{I}_M \otimes \mathbf{W}_N)] \mathbf{x}}_{\mathbf{H}_{\text{DS}}: \text{Delay-sequency effective channel matrix}} \\
& \underbrace{+ [(\mathbf{I}_M \otimes \mathbf{W}_N) \mathbf{P}^T (\beta_{\text{tx}} \alpha_{\text{rx}} \mathbf{R}_{\text{cp}} \Theta_{\text{pn}}^{\text{rx}} \Theta_{\text{cfo}}^* \mathbf{H} \Theta_{\text{pn}}^{\text{tx}} \mathbf{A}_{\text{cp}} + \alpha_{\text{tx}}^* \beta_{\text{rx}} \mathbf{R}_{\text{cp}} \Theta_{\text{pn}}^{\text{rx}} \Theta_{\text{cfo}}^* \mathbf{H}^* \Theta_{\text{pn}}^{\text{tx}} \mathbf{A}_{\text{cp}}) \mathbf{P} (\mathbf{I}_M \otimes \mathbf{W}_N)] \mathbf{x}^*}_{\text{Conjugated signal term}} \\
& \underbrace{+ [(\mathbf{I}_M \otimes \mathbf{W}_N) \mathbf{P}^T (\alpha_{\text{rx}} \mathbf{R}_{\text{cp}} \Theta_{\text{pn}}^{\text{rx}} \Theta_{\text{cfo}}^* \mathbf{H} \mathbf{A}_{\text{cp}} + \beta_{\text{rx}} \mathbf{R}_{\text{cp}} \Theta_{\text{pn}}^{\text{rx}} \Theta_{\text{cfo}}^* \mathbf{H} \mathbf{A}_{\text{cp}})] d^{\text{tx}} \mathbf{1}_{NM}}_{\text{DC due to Tx-DCO imposed by channel, Rx PN, and CFO}} + \underbrace{[(\mathbf{I}_M \otimes \mathbf{W}_N) \mathbf{P}^T] d^{\text{rx}} \mathbf{1}_{NM}}_{\text{DC due to Rx-DCO}} \\
& \underbrace{+ [(\mathbf{I}_M \otimes \mathbf{W}_N) \mathbf{P}^T (\alpha_{\text{rx}} \mathbf{R}_{\text{cp}} \Theta_{\text{pn}}^{\text{rx}} \Theta_{\text{cfo}}^* \mathbf{w} + \beta_{\text{rx}} \mathbf{R}_{\text{cp}} \Theta_{\text{pn}}^{\text{rx}} \Theta_{\text{cfo}}^* \mathbf{w}^*)]}_{\text{Noise term: Imposed by Rx-IQI, Rx-PN, and CFO}}
\end{aligned} \tag{33}$$

$$\mathbf{y}_m^{\text{HI}} = \sum_{l \in \mathcal{L}} \tilde{\mathbf{u}}_{i_{m,l}} \boxtimes \mathbf{x}_{m-1} + \mathbf{u}_{2_{m,l}} \boxtimes \mathbf{x}_{m-1}^* + \mathbf{u}_{3_{m,l}} \boxtimes \hat{\mathbf{d}}_m^{\text{tx}} + \hat{\mathbf{d}}_m^{\text{rx}} + \hat{\mathbf{w}}_m, \tag{28}$$

where  $\tilde{\mathbf{u}}_{i_{m,l}} = \mathbf{W}_N \cdot \tilde{\mathbf{g}}_{i_{m,l}}$  for  $i=1,2,3$  are the sequency spread vectors,  $\mathbf{x}_{m-1} = \mathbf{W}_N \cdot \tilde{\mathbf{x}}_{m-1}$ ,  $\hat{\mathbf{w}}_m = (\mathbf{W}_N \cdot \tilde{\mathbf{w}}_m)$ ,  $\hat{\mathbf{d}}_m^{\text{tx}} = (\mathbf{W}_N \cdot \tilde{\mathbf{d}}_m^{\text{tx}}) = [N d^{\text{tx}}, \mathbf{0}_{N-1}^T]^T$ , and  $\hat{\mathbf{d}}_m^{\text{rx}} = (\mathbf{W}_N \cdot \tilde{\mathbf{d}}_m^{\text{rx}}) = [N d^{\text{rx}}, \mathbf{0}_{N-1}^T]^T$ . Defining the sequency spread matrices as  $\mathbf{U}_{i_{m,l}} = \mathbf{W}_N \tilde{\mathbf{G}}_{i_{m,l}} \mathbf{W}_N$ , where  $\tilde{\mathbf{G}}_{i_{m,l}} = \text{diag}(\tilde{\mathbf{g}}_{i_{m,l}}[0], \dots, \tilde{\mathbf{g}}_{i_{m,l}}[N-1])$  for  $i=1,2,3$ , the I/O relation in (28) can be rewritten as

$$\mathbf{y}_m^{\text{HI}} = \sum_{l \in \mathcal{L}} \mathbf{U}_{1_{m,l}} \mathbf{x}_{m-1} + \mathbf{U}_{2_{m,l}} \mathbf{x}_{m-1}^* + \mathbf{U}_{3_{m,l}} \hat{\mathbf{d}}_m^{\text{tx}} + \hat{\mathbf{d}}_m^{\text{rx}} + \hat{\mathbf{w}}_m. \tag{29}$$

The I/O relation given in (29) is further shown in Fig. 3 for  $N=M=8$  and  $l_{\text{max}}=2$ . Since we have  $\hat{\mathbf{d}}_0^{\text{tx}} = \hat{\mathbf{d}}_1^{\text{tx}} = \dots = \hat{\mathbf{d}}_{M-1}^{\text{tx}}$  and  $\hat{\mathbf{d}}_0^{\text{rx}} = \hat{\mathbf{d}}_1^{\text{rx}} = \dots = \hat{\mathbf{d}}_{M-1}^{\text{rx}}$ , the multiplication terms  $\mathbf{U}_{3_{m,l}} \hat{\mathbf{d}}_m^{\text{tx}} = \mathbf{U}_{3_{m,l}} \hat{\mathbf{d}}_i^{\text{tx}}$  for  $i=0, \dots, M-1$  are used for the sake of presentation in the third term in Fig. 3. In other words, each row of the  $NM \times NM$  dimensional matrix in the third term can be written in different forms by considering the mentioned property; however, for all representation of the matrix, its bandwidth, i.e., the maximum number of non-zero entries in each of its rows, becomes  $N(l_{\text{max}}+1)$ .

#### D. Matrix-Form I/O Relations in Time, DT, and DS Domains in Terms of the Effective Channel Matrices

Because of the ZP symbols used in DS domain at Tx, the IBI is removed [7] and as a result the I/O relation in time domain in terms of the transmitted hardware impaired samples  $\mathbf{s}^{\text{HI}}$  and banded channel matrix  $\mathbf{H} \in \mathbb{C}^{(NM+l_{\text{max}}) \times (NM+l_{\text{max}})}$  is given as

$$\mathbf{r} = \mathbf{H} \mathbf{s}^{\text{HI}} + \mathbf{w}. \tag{30}$$

Accordingly, the I/O relation in time domain for the input of the system before CP insertion namely  $\tilde{\mathbf{s}}$  and the output of the system after CP removal namely  $\tilde{\mathbf{r}}^{\text{HI}}$ , as depicted in Fig. 2, in terms of the effective channel matrix  $\mathbf{G} \in \mathbb{C}^{NM \times NM}$  and noise vector  $\tilde{\mathbf{w}}$  is represented as

$$\tilde{\mathbf{r}}^{\text{HI}} = \mathbf{G} \tilde{\mathbf{s}} + \tilde{\mathbf{w}}, \tag{31}$$

where  $\mathbf{G} = \mathbf{R}_{\text{cp}} \mathbf{H} \mathbf{A}_{\text{cp}}$ .

Substituting (5) and (19) in (31), the I/O relation in DT domain is obtained as

$$\tilde{\mathbf{y}}^{\text{HI}} = \tilde{\mathbf{G}} \tilde{\mathbf{x}} + \tilde{\mathbf{w}}, \tag{32}$$

where  $\tilde{\mathbf{G}} = \mathbf{P}^T \mathbf{R}_{\text{cp}} \mathbf{H} \mathbf{A}_{\text{cp}} \mathbf{P}$  is the block-diagonal effective channel matrix in DT domain, i.e., every block of samples can be independently analyzed in DT domain.

To obtain the I/O relation in DS domain, 8 substitutions are done from (8) to (21) as follows. First, (8) is substituted in (9), then (9) in (10), then (10) in (12), then (12) in (13), then (13) in (14), then (14) in (17), then (17) in (18), and finally by putting (18) in (21), the matrix form of the I/O relation in DS domain is obtained as (33), where,  $\Theta_{\text{pn}}^{\text{tx}} = \text{diag}(\theta_{\text{pn}}^{\text{tx}})$ ,  $\Theta_{\text{pn}}^{\text{rx}} = \text{diag}(\theta_{\text{pn}}^{\text{rx}})$ , and  $\Theta_{\text{cfo}} = \text{diag}(\theta_{\text{cfo}})$  denote the Tx-PN, Rx-PN, and CFO phase matrices, respectively.

#### E. Some Discussions about the I/O Relations, Noise, and Sequency Interference in DS Domain

The I/O relation in (33) gives useful insights and information in terms of the DS channel matrix, interference, noise, and the state of the received signal to interference and noise as the related terms are separate in (33). Accordingly, some conclusions are discussed in what follows.

i) In the first term in (33), the DS channel matrix under HIs named as  $\mathbf{H}_{\text{DS}}$  is a diagonal matrix whose bandwidth is equal to  $N(l_{\text{max}}+1)$ . Accordingly, the maximum number of non-zero entries over the number of all entries in  $\mathbf{H}_{\text{DS}}$  is equal to  $N(l_{\text{max}}+1)/(NM+l_{\text{max}})^2$  approximated as  $((l_{\text{max}}+1)/NM^2) \ll 1$  revealing the fact that the effective channel matrix in DS domain has a sparse representation.

ii) The second term in (33) represents the self-interference in terms of the conjugated symbols in DS domain. In analogy to self-degradation and the mirror Doppler interference (MDI) introduced along the Doppler axis in DD domain in the IQI-OTFS systems [17], the channel impaired symbols in DS domain deal with sequency interference in IQI-OTSM. As depicted in Fig. 4, the sequency values of the channel impaired symbols and intercurrent conjugated symbols are the same. Therefore, in contrary to IQI-OTFS in which we have MDI, i.e., intercurrent conjugated symbols concurrently appear at symmetric Doppler taps  $-k_i$  and  $k_i$ , they interfere with the channel impaired symbols fully overlapping at the same sequency taps in IQI-OTSM for all delay taps, which may lead to degradation of signal power. In other words, IQI in OTSM transceivers redounds to self-conjugated sequency

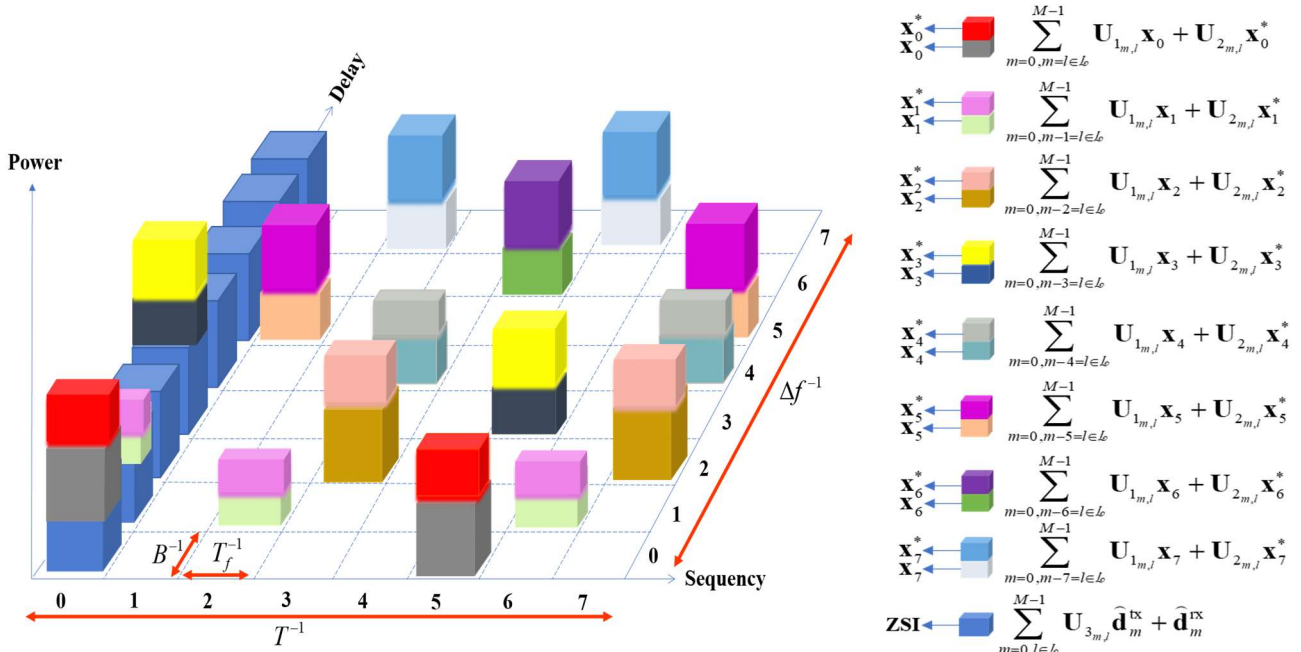


**Fig. 4.** Illustration of SCS and ZSI in OTSM in the presence of Tx/Rx IQI and Tx/Rx DCO.

interference (SCSI) of the symbols along all their sequences as illustrated in Fig. 4.

iii) The third and fourth terms in (33) correspond to the Tx-DCO and Rx DCO, respectively, which appear as DC signals in DS domain. As depicted in Fig. 4, Tx/Rx DCO interferes with only the zero sequence of the channel impaired symbols over all delay taps, which is named zero sequence interference (ZSI).

iv) The fifth term in (33), which is also given as  $\hat{\mathbf{w}}$  in the vector form of (29), describes the noise vector in DS domain. The covariance matrix of  $\hat{\mathbf{w}}$  is obtained as

$$\text{cov}(\hat{\mathbf{w}}) = (1 + \cos(2\omega) + g_{\text{rx}}^2(1 - \cos(2\omega + \varphi_{\text{rx}})))\sigma_o^2/2\mathbf{I}_{NM}, \quad (34)$$

where,  $\omega = 2\pi f_o q + \theta_{\text{pn}}^{\text{rx}}[q]$  for  $q = 0, \dots, NM - 1$  corresponds to the CFO and Rx-PN; please refer to Appendix A to see the proof. Accordingly, we can conclude Lemma 1 as

**Lemma 1:** Noise is statistically white Gaussian in DS domain under Rx-IQI, Rx-DCO, Rx-PN, CFO, and STO.

*Proof:* Please refer to Appendix A to see the proof.

Accordingly, under the condition with no CFO, Rx-PN, and Rx-IQI, namely  $f_o = 0$ ,  $\theta_{\text{pn}}^{\text{rx}}[q] = 0$ ,  $\varphi_{\text{rx}} = 0^\circ$ , and  $g_{\text{rx}} = 1$ , the noise amplification is ideally obtained equal to zero in DS domain. Also, from (33) and (34), it is concluded that CFO and Rx-PN have no influence on noise in the absence of Rx-IQI; however, Rx-IQI amplifies the noise variance with a factor of  $(1 + g_{\text{rx}}^2(1 - \cos(\varphi_{\text{rx}})))/2$  even in the absence of Rx-PN and CFO. Therefore, under the condition that we have no CFO and Rx-PN, the amplified noise can be roughly ignored if the gain and phase imbalances are negligible; as a result, the noise in time and DS domains become identically distributed.

v) Considering an ideal system with no HIs, i.e.,  $\varphi_{\text{rx}} = \varphi_{\text{tx}} = 0^\circ$ ,  $g_{\text{tx}} = g_{\text{rx}} = 1$ ,  $d^{\text{tx}} = d^{\text{rx}} = 0$ , and  $\theta_{\text{pn}}^{\text{tx}}(t) = \theta_{\text{pn}}^{\text{rx}}(t) = f_o = 0$ , which results in  $\alpha_{\text{tx}} = \alpha_{\text{rx}} = 1$ ,  $\beta_{\text{tx}} = \beta_{\text{rx}} = 0$ , and  $\Theta_{\text{pn}}^{\text{tx}} = \Theta_{\text{pn}}^{\text{rx}} = \Theta_{\text{cfo}} = \mathbf{I}_{NM+l_{\text{max}}}$ ,

the I/O relation in (33) is simplified to (35), which was first obtained by Thaj *et al.* in [7].

$$\mathbf{y} = (\mathbf{I}_M \otimes \mathbf{W}_N) \mathbf{P}^T \mathbf{G} \mathbf{P} (\mathbf{I}_M \otimes \mathbf{W}_N) \mathbf{x} + (\mathbf{I}_M \otimes \mathbf{W}_N) \mathbf{P}^T \mathbf{R}_{\text{cp}} \mathbf{w}. \quad (35)$$

vi) Considering only Rx-IQI and no other HI, i.e.,  $\varphi_{\text{tx}} = 0^\circ$ ,  $g_{\text{tx}} = 1$ ,  $d^{\text{tx}} = d^{\text{rx}} = 0$ , and  $\theta_{\text{pn}}^{\text{tx}}(t) = \theta_{\text{pn}}^{\text{rx}}(t) = f_o = 0$ , which results in  $\alpha_{\text{tx}} = 1$ ,  $\beta_{\text{tx}} = 0$ , and  $\Theta_{\text{pn}}^{\text{tx}} = \Theta_{\text{pn}}^{\text{rx}} = \Theta_{\text{cfo}} = \mathbf{I}_{NM+l_{\text{max}}}$ , the I/O relation in (33) is simplified to (36), which was first obtained by Neelam *et al.* in [24].

$$\begin{aligned} \mathbf{y}^{\text{HI}} = & [\alpha_{\text{rx}} (\mathbf{I}_M \otimes \mathbf{W}_N) \mathbf{P}^T \mathbf{R}_{\text{cp}} \mathbf{H} \mathbf{A}_{\text{cp}} \mathbf{P} (\mathbf{I}_M \otimes \mathbf{W}_N)] \mathbf{x} + \\ & [\beta_{\text{rx}} (\mathbf{I}_M \otimes \mathbf{W}_N) \mathbf{P}^T \mathbf{R}_{\text{cp}} \mathbf{H} \mathbf{A}_{\text{cp}} \mathbf{P} (\mathbf{I}_M \otimes \mathbf{W}_N)] \mathbf{x}^* + \\ & [(\mathbf{I}_M \otimes \mathbf{W}_N) (\alpha_{\text{rx}} \mathbf{P}^T \mathbf{R}_{\text{cp}} \mathbf{w} + \beta_{\text{rx}} \mathbf{P}^T \mathbf{R}_{\text{cp}} \mathbf{w}^*)]. \end{aligned} \quad (36)$$

vii) Considering only Tx/Rx IQI with no other HI, i.e.,  $d^{\text{tx}} = d^{\text{rx}} = 0$ , which results in  $\tilde{\mathbf{d}}^{\text{tx}} = \tilde{\mathbf{d}}^{\text{rx}} = \mathbf{0}_{NM}$ , the I/O relation in terms of sequence spread matrices in (29) is simplified to (37), which was first obtained by Neelam *et al.* in [25].

$$\mathbf{y}_m^{\text{HI}} = \sum_{l \in L} \mathbf{U}_{1m,l} \mathbf{x}_{m-1} + \mathbf{U}_{2m,l} \mathbf{x}_{m-1}^* + \hat{\mathbf{w}}_m. \quad (37)$$

## V. PERFORMANCE EVALUATION

In this section, we assess the performance of OTSM under different HIs both individually and by considering their joint effects through simulations carried out with MATLAB. In addition, we examine the BER performance for different detectors, QAM orders, and mobility speeds. We employ matched filtering Gauss Seidel (MFGS) detector unless otherwise is stated. The power delay profile (PDP) in dB and tap delays of standard Extended Vehicular A (EVA) channel model [28] are used along with other parameter settings given in Table I. Also, uniform Doppler shifts are considered over each path with fractional values of delay and Doppler. In all simulation studies,  $10^5$  frames are transmitted to calculate the BER at each SNR point.

TABLE I  
SIMULATION PARAMETERS

$[M, N], B$ (MHz), $P$	$[64, 64], 10, 9$
Pilot Power	2.5, 3, 3.5
Speed (Kph)	120, 500, 1000
Modulation	4-QAM, 16-QAM, 64-QAM
$f_c$ (GHz)	$[20, 28, 35, 60]$
PDP	$[0, -1.5, -1.4, -3.6, -0.6, -9.1, -7, -12, -16.9]$
Tap delay (ns)	$[0, 30, 150, 310, 370, 710, 1090, 1730, 2510]$

#### A. Performance Evaluation under Tx/Rx DCO

In Fig. 5, the BER performance of OTSM is compared with plain SC and OTFS under Tx/Rx DCO with excess pilot power of  $\beta = 3$  dB. Also, the performance of OTFS by using the scheme addressed in [20] for Tx/Rx DCO compensation is further illustrated along with the performance of ideal system experiencing no HIs. It is observed that OTSM outperforms plain SC and performs as well as uncompensated OTFS; however, the performance floors because of Tx/Rx DCO in both OTSM and uncompensated OTFS. On the other hand, the compensated OTFS performs close to ideal system. Therefore, Tx/Rx DCO severely degrades the performance and its severity becomes drastic for high values of the Tx/Rx DCO. For example, at an SNR value of 28 dB, the BER of OTSM is 116.7 times less than that of SC; however, it is 1500 times more than that of ideal system. Therefore, Tx/Rx DCO compensation is needed in mmWave OTSM systems.

#### B. Performance Evaluation under Tx/Rx IQI and PAN

In Fig. 6, the BER performance of OTSM is compared with plain SC and OTFS in the presence of Tx/Rx IQI and PAN with excess pilot power of  $\beta = 2.5$  dB. In the cases of OTSM and OTFS with HIs, the Tx/Rx IQI in OTSM and OTFS are compensated through the method presented in [25] and [22], respectively; however, the transmitted signal undergoes PAN. To evaluate the effect of PAN, we set inappropriate values for non-linear memory depth  $M_\rho$  and non-linearity order  $N_\rho$  as given in (12) not to remove the effects of PAN from the transmitted signal. Also, in the case of OTFS with HIC, the Tx-IQI and PAN are jointly compensated through digital predistortion method presented in [18] and Rx-IQI is compensated by using the scheme proposed in [19]. It is observed that OTSM outperforms plain SC and its performance is as well as OTFS; however, both OTSM and OTFS floor due to uncompensated PAN. Also, the performance degrades drastically in OTSM and OTFS by increasing the PAN. On the other hand, the compensated OTFS performs close to ideal system involving no HIs. For instance, at an SNR value of 28 dB, the BER of OTSM is 20 times less than that of SC; however, it is 250 times more than that of ideal system. Therefore, PAN compensation is needed in mmWave OTSM systems.

#### C. Performance Evaluation under Tx/Rx PN

In Fig. 7, the BER performance of OTSM is compared with plain SC and OTFS in the presence of Tx/Rx PN for different carrier frequencies. To show the amount of PN loss and the necessity of PN compensation, we further examine the BER performance of ideal system under no HIs as well as the

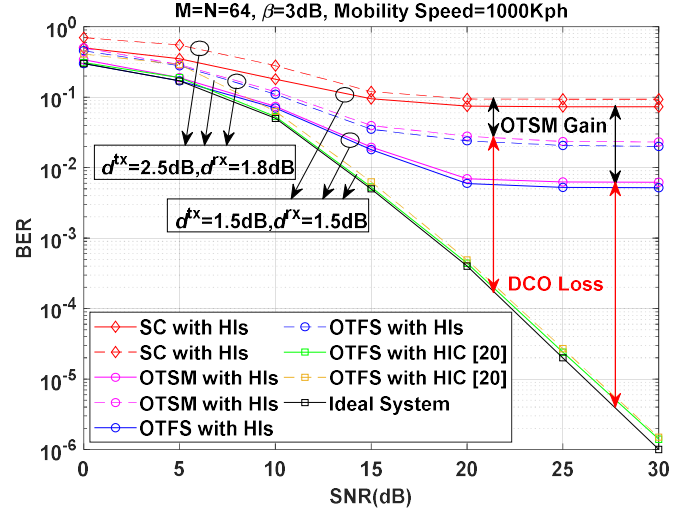


Fig. 5. The BER performance in the presence of Tx/Rx DCO.

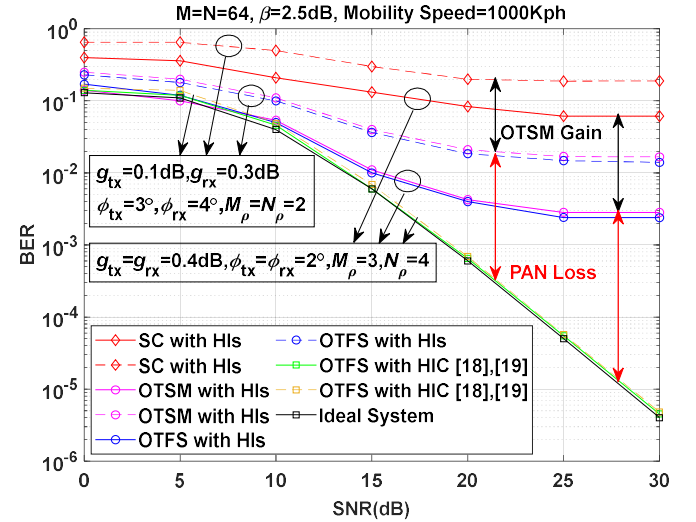


Fig. 6. The BER performance in the presence of Tx/Rx IQI and PAN.

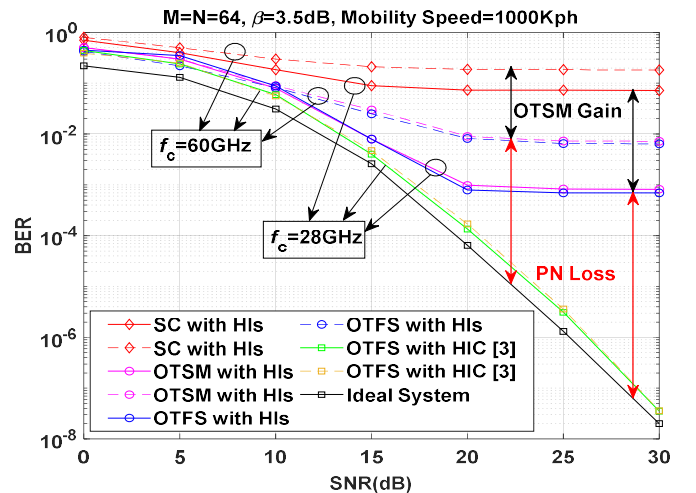


Fig. 7. The BER performance in the presence of Tx/Rx PN.

performance of OTFS with HIC based on the method proposed in [3]. As clearly seen, under Tx/Rx PN, OTSM surpasses plain SC and it achieves performance gain close to uncompensated OTFS for different carrier frequencies; however, because of PN, increasing the carrier frequency increases the error floor in uncompensated OTFS and OTSM for SNR values more than 20 dB. On the other hand, the performance of OTFS after Tx/Rx PN compensation is close to ideal system. For example, at an SNR value of 29 dB, the BER of OTSM is 117 times less than that of SC; however, it is 11667 times more than ideal system revealing the imperative lack of PN compensation in mmWave OTSM systems.

#### D. Performance Evaluation under CFO

In Fig. 8, we show the BER performance of OTSM under CFO. To show the necessity of CFO compensation in OTSM, we set an ideal system with no CFO and an OTFS system in which the method proposed in [21] is deployed to compensate the CFO as the benchmarks. As clearly seen, OTSM outperforms plain SC and performs close to uncompensated OTFS system under CFO. However, due to the CFO impairment, the BER floors for SNR values more than 20 dB and, by increasing the CFO, the error floor raises making the system performance unacceptable in practice. On the other hand, the performance of OTFS with HIC closely matches with ideal system for different values of CFO. For example, at an SNR value of 27.8 dB, OTSM achieves 15 times gain and 2750 time loss in comparison with the ideal system. Therefore, CFO severely degrades the performance and CFO compensation is essentially needed in mmWave OTSM systems.

#### E. Performance Evaluation under Tx/Rx IQI and STO

In Fig. 9, we examine the BER performance of OTSM in the presence of Tx/Rx IQI under STO. To show the necessity of Tx/Rx IQI compensation under STO in OTSM, we compensate the Tx/Rx IQI in OTSM in the absence of STO based on the method addressed in [25]. Also, an ideal system with no HIs and an OTFS system in which the method proposed in [22] is utilized to compensate Tx/Rx IQI in the presence of STO are considered as the benchmarks. Furthermore, as this simulation study aims at assessing the STO effect, we set inappropriate values for  $I_1$ ,  $I_2$ , the base-point of interpolant, and fractional interval vectors of the interpolating filter as given in (17), not to compensate STO at the receiver. As obviously shown, OTSM under STO outperforms plain SC while exhibiting close to uncompensated OTFS system for different scenarios. However, because of the STO impairment, the BER floors for SNR values more than 20 dB and by increasing the severity of STO, the error floor raises leading to an indign system performance in practice. On the other hand, the OTFS with HIC performs close to ideal system. For instance, at an SNR value of 27.8 dB, OTSM achieves 8 times gain and  $35 \times 10^4$  times loss compared to plain SC and ideal system, respectively. Therefore, STO impairs the performance and HIC in the presence of STO is basically required in mmWave OTSM systems.

#### F. Performance Evaluation under Tx/Rx IQI, Tx/Rx DCO, Tx/Rx PN, PAN, CFO, and STO for Different QAM Orders, Mobility Speeds, and Detectors

In Fig. 10, we evaluate the overall BER performance of

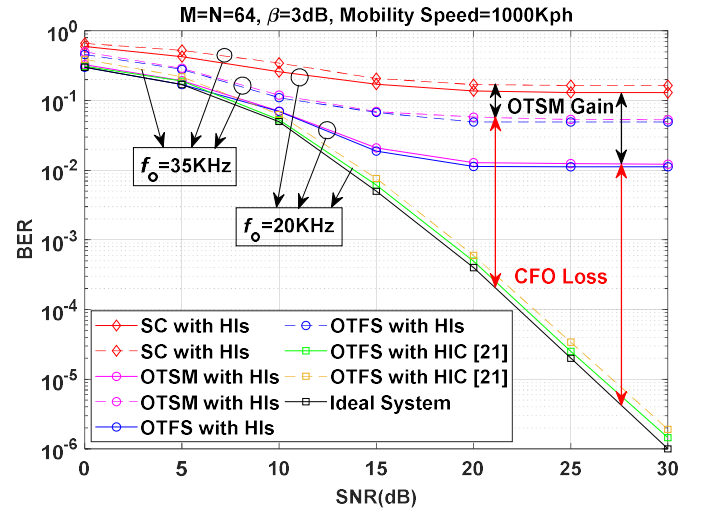


Fig. 8. The BER performance in the presence of CFO.

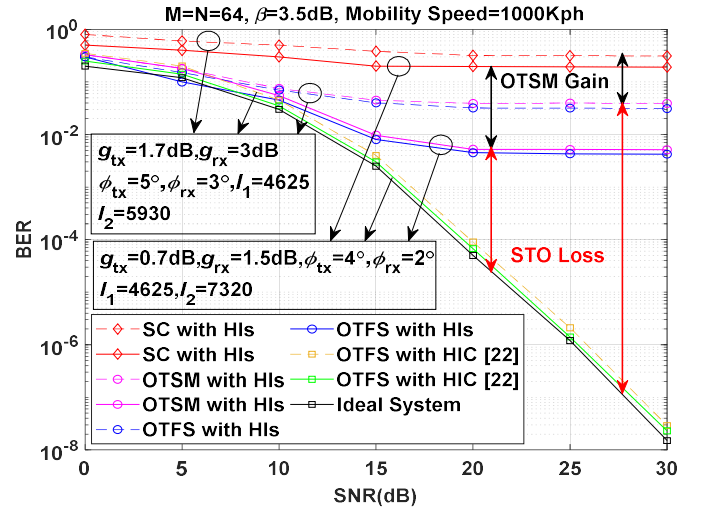


Fig. 9. The BER performance in the presence of Tx/Rx IQI and STO

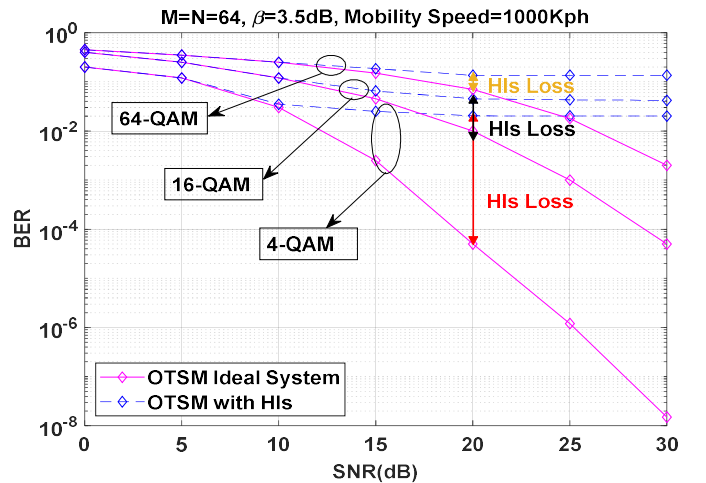


Fig. 10. The BER performance under HIs for varying QAM order.

OTSM by incorporating all HIs for different QAM orders. It is observed that 4-QAM performs better than 16-QAM and 64-QAM constellations. Also, for SNR values more than 10 dB, the BER floors. Although HIs loss decreases for higher orders of QAM, the error floor increases to the value being unacceptable for mmWave practical systems.

In Fig. 11, we examine the overall BER performance of OTSM by considering all HIs for different mobility speeds. It is observed that increasing the mobility speed does not increase the error significantly revealing the robustness and potential of OTSM under HIs in high mobility scenarios. However, the amount of error floor is not acceptable in practice and the HIs loss significantly increases by raising the SNR. For example, at an SNR value of 28 dB, the BER of OTSM under HIs is  $2 \times 10^5$  times more than that of ideal system at a mobility speed of 1000 Kph with 4-QAM constellation and  $\beta = 3.5$  dB.

In Fig. 12, we assess the overall BER performance of OTSM under HIs for MFGS, linear minimum mean square error (LMMSE), and single-tap detectors. It is clearly seen that in both cases of ideal system and under HIs, MFGS detector outperforms both LMMSE and single tap methods of detection. Although Tx/Rx IQI is compensated based on the method proposed in [25], all of the detectors floor for SNR values more than 15 dB due to other HIs. This demonstrates the essential need to HIC in terms of Tx/Rx DCO, Tx/Rx PN, PAN, CFO, and STO in mmWave OTSM systems.

From the comparison of results in Figs. 5 to 12, we conclude that adopting 4-QAM constellation with MFGS detector provides significantly higher performance in OTSM systems compared to plain SC under HIs over DSCs with high mobilities; however, HIs severely degrade the BER performance. The comparison of BER loss compared to ideal system as well as OTSM gain in comparison with plain SC under different HIs have been further shown in Table I at a mobility speed of 1000 Kph employing 4-QAM constellation and MFGS detector,  $\beta = 3.5$ ,  $f_c = 35$  GHz,  $f_o = 25$  kHz,  $I_1 = 4867$ ,  $I_2 = 5432$ ,  $M_p = 3$ ,  $N_p = 4$ ,  $\phi_{tx} = 3^\circ$ ,  $\phi_{rx} = 4^\circ$ ,  $g_{tx} = 1.5$  dB,  $g_{rx} = 1.2$  dB,  $d^{tx} = 1.3$ , and  $d^{rx} = 1.8$  dB. As listed in Table II, by raising the SNR, the BER loss increases. Also, at SNR value of 20 dB, the BER of OTSM under all HIs is 87.52% less than that of plain SC; however, it is 99.86% more than that of ideal system. Therefore, HIC is necessarily needed in mmWave OTSM systems.

## VI. CONCLUSION AND FUTURE INSIGHTS

Derivation of the I/O relation under HIs is a prerequisite for HIC being an essential design step in mmWave wireless communication systems. In this paper, we have derived the discrete-time baseband signal model and the I/O relations for OTSM system in time, DT, and DS domains by considering Tx/Rx IQI, Tx/Rx DCO, Tx/Rx PN, PAN, CFO, and STO. It has been shown that the I/O relations presented in previous works on this topic are all obtained as the special cases from our proposed comprehensive I/O relations. Thanks to our proposed I/O relation in DS domain, we have analytically demonstrated that noise is additive white Gaussian and the effective channel is sparse in DS domain under mentioned

TABLE II  
BER LOSS AND OTSM GAIN COMPARISON UNDER  
DIFFERENT HIs

HI	BER Loss SNR=15 dB	BER Loss SNR=20 dB	OTSM Gain SNR=20 dB
Tx/Rx IQI [25]	79.35%	97.54%	93.46%
Tx/Rx DCO	72.54%	95.43%	91.45%
PAN	38.64%	85.65%	96.58%
Tx/Rx PN	69.48%	93.56%	98.85%
CFO	65.82%	89.12%	89.23%
STO	81.45%	98.12%	95.83%
Overall	91.39%	99.86%	87.52%

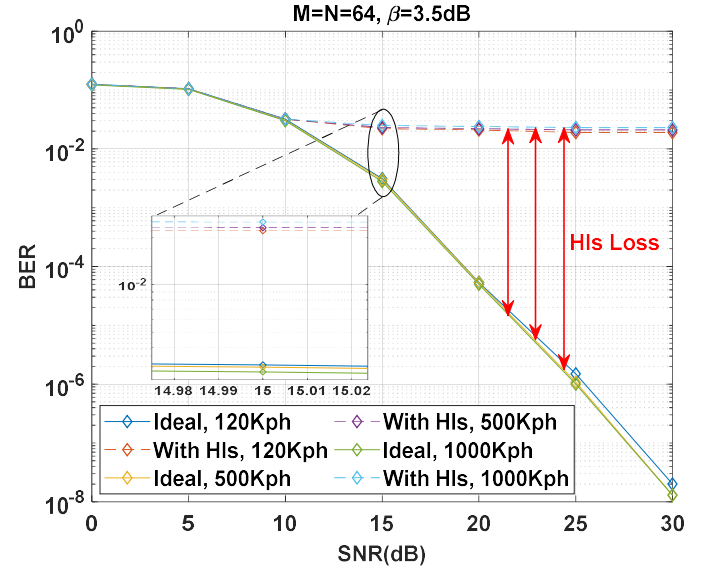


Fig. 11. The BER performance under HIs for varying mobility speed.

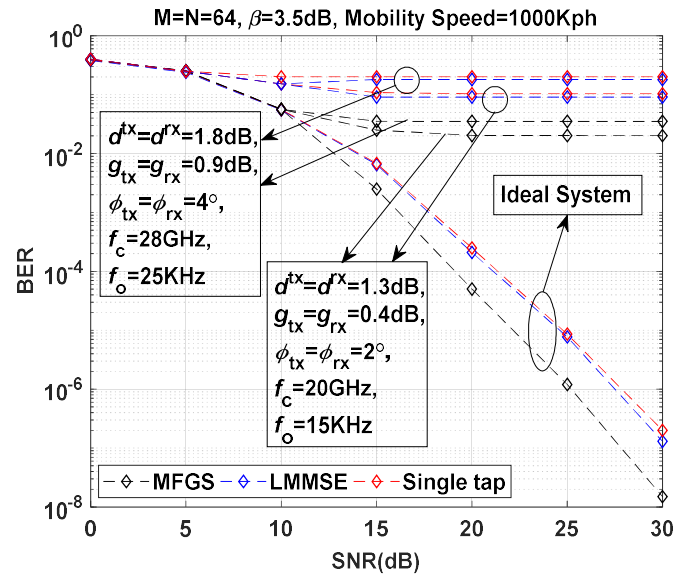


Fig. 12. The BER performance under HIs for different detectors.



given in (33) is equal to

$$\hat{\mathbf{w}} = (\mathbf{I}_M \otimes \mathbf{W}_N) \mathbf{P}^T (\alpha_{\text{rx}} \mathbf{R}_{\text{cp}} \mathbf{\Theta}_{\text{pn}}^{\text{rx}} \mathbf{\Theta}_{\text{cfo}} \mathbf{w} + \beta_{\text{rx}} \mathbf{R}_{\text{cp}} \mathbf{\Theta}_{\text{pn}}^{\text{rx}} \mathbf{\Theta}_{\text{cfo}}^* \mathbf{w}^*), \quad (39)$$

which is a linear combination of Gaussian vectors  $\mathbf{w}$  and  $\mathbf{w}^*$ . Therefore,  $\hat{\mathbf{w}}$  stays Gaussian and as  $\mathbf{w}$  is zero-mean,  $\hat{\mathbf{w}}$  becomes zero-mean [32]. In addition, by considering the unitary property of WHT, the covariance matrix of  $\hat{\mathbf{w}}$  is given as (40) where  $E(\cdot)$  denotes the mathematical expectation,  $\text{Re}(\cdot)$  denotes the real part, and  $\mathbf{K} = \text{diag}(e^{-j2\omega})$  in which  $\omega = 2\pi f_o q + \theta_{\text{pn}}^{\text{rx}}[q]$  for  $q = 0, \dots, NM - 1$ . Since the Gaussian vector  $\hat{\mathbf{w}}$  is zero-mean and the covariance matrix of  $\hat{\mathbf{w}}$  is also diagonal,  $\hat{\mathbf{w}}$  is therefore white Gaussian [32].

## REFERENCES

- [1] Y. Zhou, et al., "Overview and performance analysis of various waveforms in high mobility scenarios," 2023, arXiv:2302.14224. [online]. Available: <https://doi.org/10.48550/arXiv.2302.14224>.
- [2] Z. Sha and Z. Wang, "Channel estimation and equalization for terahertz receiver with RF impairments," *IEEE J. Sel. Areas. Commun.*, vol. 39, no. 6, pp. 1621-1635, June 2021.
- [3] Y. Bello, et al., "OTFS waveform with phase noise in sub-THz," in *2022 IEEE 96th Veh. Technol. Conf. (VTC2022-Fall)*, London, United Kingdom, 2022, pp. 1-5.
- [4] G. D. Surabhi, et al., "OTFS modulation with phase noise in mm-wave communications," in *2019 IEEE 89th Veh. Technol. Conf. (VTC2019-Spring)*, Kuala Lumpur, Malaysia, 2019, pp. 1-5.
- [5] M. Saad, et al., "Single carrier with index modulation for low-power terabit systems," in *2019 IEEE Wirel. Commun. Netw. Conf. (WCNC)*, Marrakesh, Morocco, 2019, pp. 1-7.
- [6] T. Thaj and E. Viterbo, "Orthogonal time sequency multiplexing modulation," in *Proc. IEEE Wirel. Commun. Netw. Conf. (WCNC)*, 2021, pp. 1-7.
- [7] T. Thaj, et al., "Orthogonal time sequency multiplexing modulation: Analysis and low-complexity receiver design," *IEEE Trans. Wirel. Commun.*, vol. 20, no. 12, pp. 7842-7855, Dec. 2021.
- [8] R. Hadani, et al., "Orthogonal time frequency space modulation," in *Proc. IEEE Wirel. Commun. Netw. Conf. (WCNC)*, 2017, pp. 1-6.
- [9] H. Lu, L. Zhang, X. Chen and Z. Wu, "Recursive carrier interferometry aided high data rate OFDM systems with PAPR suppression, phase noise rejection, and carrier frequency offsets compensation," *IEEE Trans. Veh. Technol.*, vol. 68, no. 4, pp. 3655-3671, April 2019.
- [10] A. Tarighat and A. H. Sayed, "Joint compensation of transmitter and receiver impairments in OFDM systems," *IEEE Trans. Wirel. Commun.*, vol. 6, no. 1, pp. 240-247, Jan. 2007.
- [11] L. Chen, A. G. Helmy, G. Yue, S. Li and N. Al-Dhahir, "Performance analysis and compensation of joint TX/RX I/Q imbalance in differential STBC-OFDM," *IEEE Trans. Veh. Technol.*, vol. 66, no. 7, pp. 6184-6200, July 2017.
- [12] Y. Meng, W. Zhang, W. Wang and H. Lin, "Joint CFO and I/Q imbalance estimation for OFDM systems exploiting constant modulus subcarriers," *IEEE Trans. Veh. Technol.*, vol. 67, no. 10, pp. 10076-10080, Oct. 2018.
- [13] X. Cheng and Z. Luo, "Compensation of transmitter I/Q imbalance in millimeter-wave SC-FDE systems," *IEEE Trans. Veh. Technol.*, vol. 66, no. 5, pp. 4472-4476, May 2017.
- [14] F. Mkadem, et al., "Complexity reduced Volterra series model for power amplifier digital predistortion," *Analog Integr. Circuits Signal Process.*, vol. 79, pp. 331-343, Feb. 2014.
- [15] A. Chung, et al., "IQ imbalance compensation and digital predistortion for mm-wave transmitters using reduced sampling rate observations," *IEEE Trans. Microw. Theory Tech.*, vol. 66, no. 7, pp. 3433-3442, July 2018.
- [16] A. Tusha, et al., "Performance analysis of OTFS under in-phase and quadrature imbalance at transmitter," *IEEE Trans. Veh. Technol.*, vol. 70, no. 11, pp. 11761-11771, Sep. 2021.
- [17] A. Tusha, et al., "Index modulation-aided IQ imbalance compensator for OTFS communications systems," in *Proc. IEEE Wirel. Commun. Netw. Conf. (WCNC)*, 2022, pp. 2178-2183.
- [18] S. G. Neelam and P. R. Sahu, "Error performance of OTFS in the presence of IQI and PA nonlinearity," in *Proc. Nat. Conf. Commun. (NCC)*, Kharagpur, India, 2020, pp. 1-6.
- [19] S. G. Neelam and P. R. Sahu, "Channel estimation and data detection of OTFS system in the presence of receiver IQ imbalance," in *Proc. Nat. Conf. Commun. (NCC)*, 2021, pp. 1-6.
- [20] S. G. Neelam and P. R. Sahu, "Digital compensation of IQ imbalance, DC offset for zero-padded OTFS systems," *IEEE Commun. Lett.*, vol. 26, no. 10, pp. 2450-2454, Oct. 2022.
- [21] S. G. Neelam and P. R. Sahu, "Analysis, estimation and compensation of hardware impairments for CP-OTFS systems," *IEEE Wirel. Commun. Lett.*, vol. 11, no. 5, pp. 952-956, May 2022.
- [22] S. G. Neelam and P. R. Sahu, "Joint compensation of TX/RX IQ imbalance and channel parameters for OTFS systems under timing offset," in *2023 Nat. Conf. Commun. (NCC)*, Guwahati, India, 2023, pp. 1-5.
- [23] M. Bayat and A. Farhang, "Time and frequency synchronization for OTFS," *IEEE Wirel. Commun. Lett.*, vol. 11, no. 12, pp. 2670-2674, Dec. 2022.
- [24] S. G. Neelam and P. R. Sahu, "Estimation and compensation of IQ imbalance for OTSM systems," *IEEE Wirel. Commun. Lett.*, vol. 11, no. 9, pp. 1885-1889, Sep. 2022.
- [25] S. G. Neelam and P. R. Sahu, "Joint compensation of Tx/Rx IQ imbalance and channel parameters for OTSM systems," *IEEE Commun. Lett.*, vol. 27, No. 3, pp. 976-980, Mar. 2023.
- [26] T. Thaj and E. Viterbo, "Low complexity iterative rake decision feedback equalizer for zero-padded OTFS systems," *IEEE Trans. Veh. Technol.*, vol. 69, no. 12, pp. 15606-15622, Dec. 2020.
- [27] D. Tse and P. Viswanath, *Fundamentals of Wireless Communication*, 3rd ed. Cambridge, U.K.: Cambridge Univ. Press, 2005.
- [28] LTE Evolved Universal Terrestrial Radio Access (E-UTRA); Base Station (BS) Radio Transmission and Reception, Standard ETSI TS, 3GPP TS 36.104 version 14.3.0 Release 14, Apr. 2017.
- [29] S. G. Neelam and P. R. Sahu, "Iterative channel estimation and data detection of OTSM with superimposed pilot scheme and PAPR analysis," *IEEE Commun. Lett.*, doi: 10.1109/LCOMM.2023.3281575.
- [30] A. K. P. and C. R. Murthy, "Orthogonal delay scale space modulation: A new technique for wideband time-varying channels," *IEEE Trans. Signal Process.*, vol. 70, pp. 2625-2638, May. 2022.
- [31] S. Liu, T. Wang and S. Wang, "Hardware impairment estimation in NB-IoT: a parallel multitask learning method," *IEEE Internet Things J.*, vol. 10, no. 8, pp. 6859-6869, Apr. 2023.
- [32] A. Papoulis and S. Unnikrishna Pillai, *Probability, Random Variables and Stochastic Processes*, 4th ed. McGraw-Hill, 2002.